



Cite this: DOI: 10.1039/d5sc09067a

All publication charges for this article have been paid for by the Royal Society of Chemistry

Deciphering the molecular origin of the 19.3 eV electronic excitation energy of H_3^+

Josene M. Toldo, ^{ab} Jakob K. Staab, ^{ac} Eduard Matito, ^{de} Cina Foroutan-Nejad ^f and Henrik Ottosson ^{*a}

The trihydrogen cation, H_3^+ , is unique in the Universe. It serves as the primary proton reservoir, driving essential astrochemical reactions, and it functions as a thermostat for giant gas planets. H_3^+ has also a remarkably low photodissociation rate, explained by its exceptionally high first electronic excitation energy (19.3 eV), which is well above the ionization energy of the much more abundant monohydrogen (13.6 eV). Herein we reveal that the key factors behind the high excitation energy of H_3^+ , and thus, its astrophotocatalytic inertness, are: (i) aromatic stabilization in its electronic ground state, (ii) antiaromatic destabilization in its first excited state, and (iii) a high nuclear-to-electronic charge ratio (+3 vs. -2). Through comparisons with analogous (isolobal) π -conjugated carbocations, we find that ground state aromatic stabilization plus excited state antiaromatic destabilization raise the excitation energy of H_3^+ by 4.8–6.0 eV. This means that for H_3^+ , the excited state antiaromatic character (which normally leads to high photoreactivity) contributes to its astrophotocatalytic inertness. Thus, only with the increase in excitation energy due to ground state aromaticity plus excited antiaromaticity can H_3^+ act as a thermostat for giant gas planets and as a proton reservoir that drives astrochemical reactions, thereby fulfilling its unique role in space.

Received 19th November 2025
 Accepted 30th December 2025

DOI: 10.1039/d5sc09067a
rsc.li/chemical-science

Introduction

Triangular H_3^+ is the most abundant polyatomic ion in the interstellar medium, where it functions as the primary interstellar acid, initiating reactions that lead to more complex molecules (Fig. 1).^{1–3} It further acts as a thermostat (coolant) in the upper atmospheres of giant gas planets,⁴ and it has been postulated that it even could have functioned as a coolant in the primordial gas (though with a different mechanism than in the giant gas planets).⁵ With three H atoms, it is the smallest molecule that exhibits aromaticity (σ -aromaticity),^{6–9} a stabilizing molecular property.¹⁰

The first electronically excited singlet states of H_3^+ , the doubly degenerate $1^1\text{E}'$ states at the equilateral triangular structure (D_{3h} symmetric), are of exceptionally high vertical energy (19.3 eV, Fig. 2),¹¹ and they are dipole-allowed and

dissociative.^{12–14} Despite this, astrochemical databases list a photodissociation rate of $4 \times 10^{-13} \text{ s}^{-1}$ or lower,^{13,15} whereby it is among the astrochemical species with lowest photodissociation rates.^{16,17} The reason is that the much more

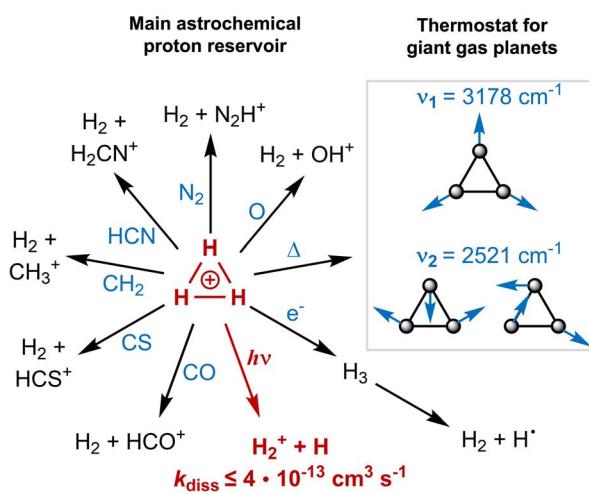


Fig. 1 A summary of the functions of H_3^+ in space, with its role as (i) primary proton reservoir initiating a number of core astrochemical reactions (typical rate constants for these reactions are $\sim 10^{-9} \text{ cm}^3 \text{ s}^{-1}$), and (ii) as a thermostat in the upper atmospheres of giant gas planets ensuring that their temperatures do not exceed a threshold.

^aDepartment of Chemistry –Ångström, Uppsala University, 751 20 Uppsala, Sweden.
 E-mail: henrik.ottosson@kemi.uu.se

^bUniversité Claude Bernard Lyon 1, ENS de Lyon, CNRS, Laboratoire de Chimie, UMR 5182, 69342, Lyon Cedex 07, France

^cDepartment of Chemistry, The University of Manchester, Oxford Road, Manchester, UK

^dDonostia International Physics Center (DIPC), 20018 Donostia, Euskadi, Spain

^eIkerbasque, Basque Foundation for Science, 48009 Bilbao, Euskadi, Spain

^fInstitute of Organic Chemistry, Polish Academy of Sciences, Warsaw, Poland

† Present Address: Department of Chemistry “Ugo Schiff”, University of Florence, 50019 Sesto Fiorentino, Italy.



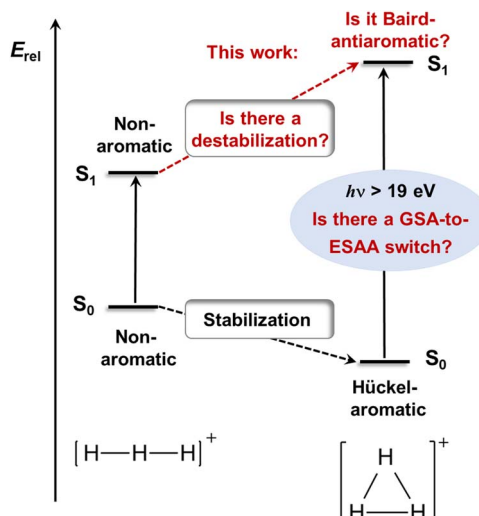


Fig. 2 Tentative changes from the nonaromatic character of linear H_3^+ in its S_0 and S_1 states to the equilateral triangular H_3^+ with a stabilizing Hückel-aromaticity in S_0 (GSA = ground state aromaticity) and a destabilizing Baird-antiaromaticity in S_1 (ESAA = excited state antiaromaticity). Factors related to our hypothesis and explored herein written in red, while known factors in black.

abundant H and H_2 , with ionization and excitation energies at 13.1–15.4 eV,^{1,18} shield H_3^+ from high-energy irradiation in the interstellar medium (ISM).^{12,13,19,20} In the ISM, H_3^+ degrades unimolecularly only when exposed to electrons ejected from other molecules or atoms upon cosmic ray ionization.^{1,13} Indeed, direct photodissociation only occurs when H_3^+ is rovibrationally excited, whereby the electronic excitation energy decreases down to 4.9 eV.^{12,13} Had it been more prone to photodissociate, this would have impaired its astrochemical and astrophysical functions, and thus, been detrimental to the development of the Universe as we presently know it. However, the molecular origins of its very high vertical excitation energy remain unknown and have never been addressed earlier. With such fundamental knowledge in hand it should also be possible to pinpoint other species of astrochemical relevance that may also exhibit unusually high first electronic excitation energies.

H_3^+ in its electronic ground state (S_0) has a D_{3h} symmetric structure^{11,21–23} with σ -aromatic character,^{6–9} in line with Hückel's $4n + 2$ rule ($n = 0, 1, 2, \dots$) as it has two σ -electrons. We now hypothesize that the counter-concept, antiaromaticity,¹⁰ is relevant for its first excited state of singlet multiplicity (S_1), and thus, its excitation energy (Fig. 2). In this context, the analogous cyclic and fully π -conjugated hydrocarbons (*i.e.*, annulenes) in their lowest excited triplet states (T_1) of $\pi\pi^*$ character follow Baird's rule,^{24–28} which tells that molecules with $4n + 2$ π -electrons are antiaromatic and destabilized in these states while those with $4n$ are aromatic and stabilized. Although derived for the T_1 state, the rule can often be extended to the lowest $\pi\pi^*$ excited state of singlet multiplicity. Thus, the exceptionally high excitation energy of H_3^+ may stem from σ -antiaromatic destabilization in S_1 (Fig. 2) combined with σ -aromatic stabilization

in S_0 , *i.e.*, a switch in character from ground state Hückel-antiaromaticity (GSA) to excited state Baird-antiaromaticity (ESAA), a GSA-to-ESAA switch in character.

Accordingly, we now investigated if the lowest excited states of H_3^+ are antiaromatic and based this assessment on quantum chemical calculations of various (anti)aromaticity descriptors. Is ESAA the factor that leads to the very high excitation energy or are there other factors? Furthermore, can knowledge gained through this investigation impact on other parts of astrochemistry? The H_3^+ cation has a 3-center 2-electron bond, a type of bonding it shares with nonclassical carbocations such as the vinyl (C_2H_3^+) and ethyl (C_2H_5^+) cations,^{29–37} species which are also of astrochemical relevance.^{38,39} One can thus argue that the findings herein can be useful to understand the astrophotophysical features of these species as well.

Computations of H_3^+ were run at the EOM-CCSD level for all species, which for H_3^+ corresponds to a full configuration interaction (FCI) calculation, *i.e.*, a numerically exact solution of the Schrödinger equation. These computations were performed using the aug-cc-pVTZ basis set of Dunning. For further computational details, see the Computational methods section and the SI.

Results and discussion

Herein, we first present and discuss results of the potential energy surfaces of the S_0 and lowest few singlet excited states, followed by assessments of the (anti)aromatic characters of these states. This allows us to get a first tentative link between the excited state surface profiles and ESAA alleviation, yet, other factors that can impact on the lowest excitation energy of H_3^+ are also identified and explored. Towards the end we compare with the analogous (isolobal) carbocations, which allows us to estimate the energetic component of a GSA-to-ESAA switch in character on the vertical excitation energy of H_3^+ .

Potential energy surfaces

According to our computations, the H–H distances of equilateral triangular H_3^+ in S_0 are 0.875 Å which is very close to the earlier computed value of 0.873 Å found with variational Born–Oppenheimer theory using explicitly correlated Gaussian functions.¹¹ The degenerate $1^1\text{E}'$ states appear vertically 19.28 eV above the S_0 state (Fig. 3A), again very similar to the reference value of 19.33 eV.¹¹ Expansion of the basis set beyond aug-cc-pVTZ has a negligible effect on the vertical excitation energy (19.2883 eV with FCI/aug-cc-pV5Z). The transition is symmetry allowed with an oscillator strength $f = 0.562$, yet, as it is well above the ionization energy of H (13.6 eV), the excitation has exceptionally low probability.

After excitation, in C_{2v} symmetry, the $1^1\text{E}'$ states split into the 2^1A_1 and 1^1B_2 states (Fig. 3B), where 2^1A_1 as S_1 dissociates to $\text{H}_2^+ + \text{H}$ while 1^1B_2 as S_1 leads to $2\text{H}(1s) + \text{H}^+$.¹⁴ These dissociative forces can be understood as a result of the Jahn–Teller theorem.⁴⁰ Along D_{3h} symmetric geometries, the degenerate 1^1E forms a conical intersection seam, which is lifted by symmetry-breaking nuclear distortions along a pair of E type vibrations, leading to electronic



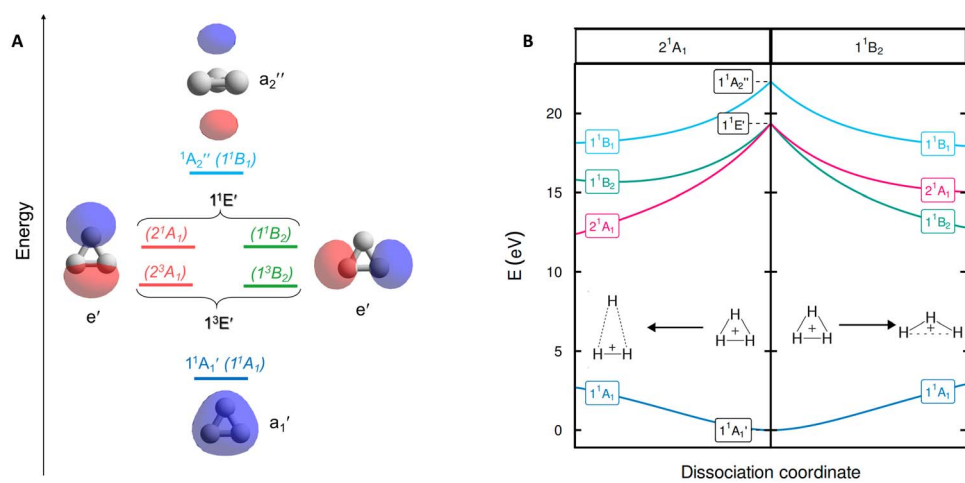


Fig. 3 (A) The three valence MOs (a'_1 and e'), the Rydberg orbital a''_2 , and the labels of the electronic states within the D_{3h} (normal print) and C_{2v} (in parenthesis and italics) point groups. (B) Potential energy surface profiles of H_3^+ from the D_{3h} symmetric S_0 equilibrium geometry along the minimum energy path of the 2^1A_1 state keeping C_{2v} symmetry to an acute isosceles triangle (left), and along the minimum energy path of the 1^1B_2 state to an obtuse isosceles triangle (right).

stabilization. We recognize that extensive vibronic coupling effects influence the excited state spectrum and that these, as well as different conical intersections, strongly impact on photochemical dissociation dynamics of H_3^+ , as has already been explored in previous studies based on highly accurate potential energy surfaces.^{13,41–46} The current work, however, does not attempt to quantitatively model neither spectroscopic data nor photodissociation rates. Instead, the objective of our study is to elucidate the origin of the unusually high electronic excitation energy of H_3^+ , which hitherto is totally unexplored.

The first triplet states (the degenerate $1^3E'$) have vertical excitation energies of 14.87 eV (Table S1) and exhibit similar dissociative behaviors as 1^1E , in line with earlier findings.⁴⁷ Lastly, the higher energy 1^1A_2 state in D_{3h} symmetry is a dissociative second-order saddle point with H–H distances of 1.620 Å. As this state involves an excitation from an a'_1 orbital to a nonbonding Rydberg-type orbital a''_2 (Fig. 3A), only one electron remains in a bonding molecular orbital (MO), which cannot counterbalance the electrostatic repulsion between three protons. For further results and discussions on this state, see Sections S1 and S2 of the SI.

Probing excited state antiaromaticity

The aromatic or antiaromatic characters of the various electronic states were determined comprehensively through use of energetic, electronic, and magnetic (anti)aromaticity descriptors (for details see Section S3 or ref. 10). Thus, we analyze changes in three of the four aspects of aromaticity, with the geometric aspect being impossible to assess due to the dissociative nature of the excited states. The energetic aspect is determined through the extra cyclic resonance energy (ECRE).^{48,49} To measure electron delocalization,⁵⁰ we use the two-center delocalization index (DI)^{51,52} and the normalized multicentre index (MCI)^{1/n}⁵³ that reflect the aromatic character.

The magnetic response properties are explored by magnetically induced current densities (MICDs), and also by nucleus independent chemical shifts (NICSS).

Although assessed in earlier reports,⁶⁻⁹ the values for σ -aromaticity of the S_0 state are discussed briefly in order to contrast the antiaromatic character of the excited states (*vide infra*). H_3^+ has two electrons and forms a 3-center 2-electron (3c-2e) bond, both in its linear and triangular structures. Therefore, the energy gain when going from the linear to the triangular structure (1.76 eV) represents the ECRE, reflecting an aromatic stabilization of cyclic H_3^+ in S_0 (Fig. 2). The topological analysis of the electron density also reveals a species that benefits from extensive 3c-2e bonding, manifested in the formation of a non-nuclear attractor (NNA) in the center (Fig. 4A), in agreement with previous works.^{7,8} Large DI values between the hydrogen atoms and the large positive MCI^{1/n} of 0.62 (Fig. 4A)⁵⁴ are also consistent with σ -aromaticity in S_0 (the MCI^{1/n} of benzene in S_0 is 0.59 (ref. 55)). Finally, H_3^+ in its S_0 state displays a diatropic MICD of 4.39 nA T⁻¹, in agreement with the NICS(0)_{zz} value of -37.1 ppm, confirming the magnetic aromaticity of H_3^+ in S_0 (see further Section S3 of the SI).

Evaluation of the potential antiaromaticity in the $1^1E'$ states of D_{3h} symmetric H_3^+ is more challenging from computational perspectives, requiring separate characterizations of the two states, the 2^1A_1 and 1^1B_2 states in C_{2v} symmetry. Indeed, our investigation offers a first exploration of whether the concept of excited-state antiaromaticity is applicable to doubly degenerate first excited states. Notably, we find that in the lowest excited state, going from the linear ($D_{\infty h}$) to the triangular geometry of H_3^+ (which is the equilibrium geometry in S_0) results in a destabilization in the lowest vertically excited singlet states by 4.19 eV (Fig. 4B). This reveals a negative ECRC indicating antiaromaticity. Thus, the stabilization in S_0 plus destabilization in $1^1E'$ (S_1) upon cyclization have implications for the vertical

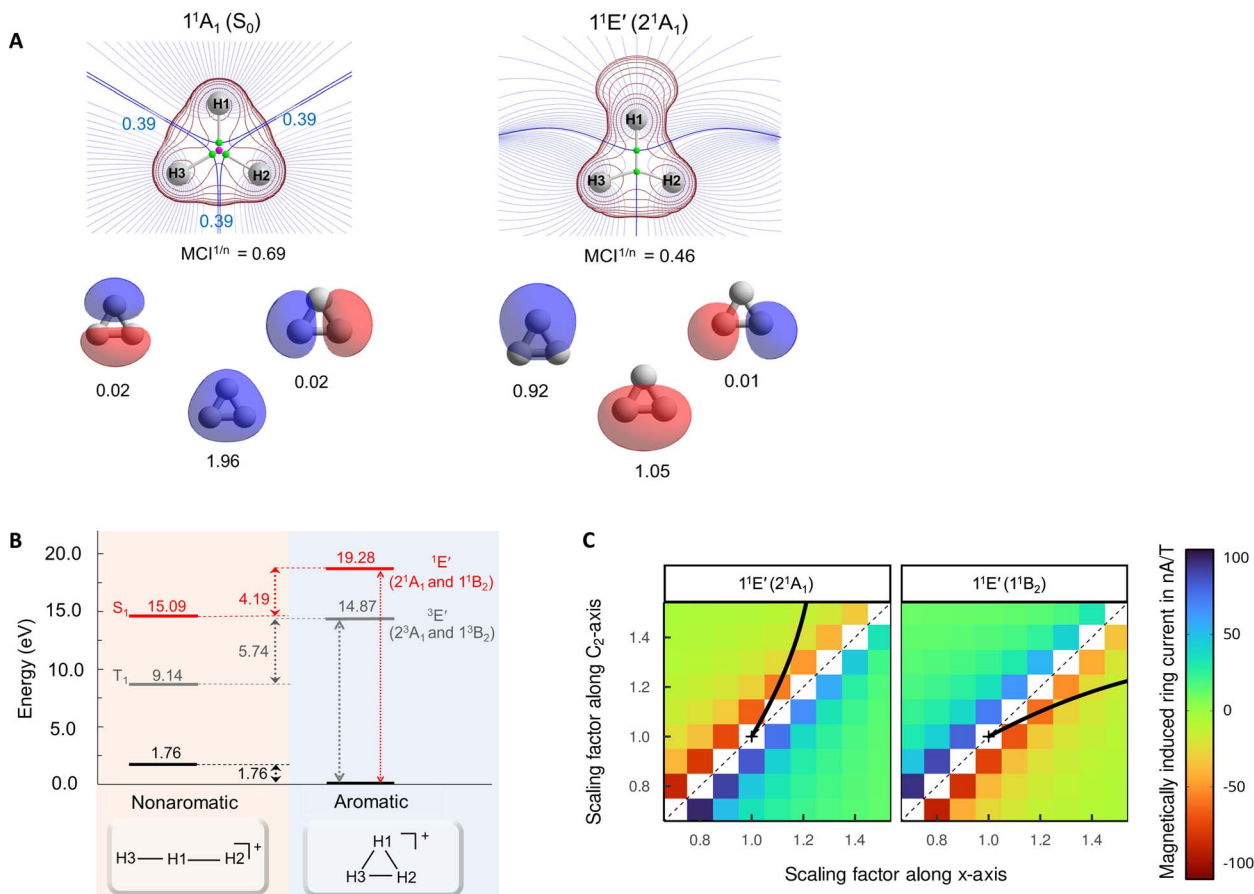


Fig. 4 (A) Topological analysis of the electron density, 2D Laplacian of the electron density (in red), and natural orbitals (with populations) for the S_0 and $1^1E'$ states, the latter labelled as 2^1A_1 and 1^1B_2 in C_{2v} symmetry. The rays of the basins drawn in blue and density gradient lines in purple. $MCI^{1/n}$ values (computed using Becke-rho's partition)⁵⁶ are given below the Laplacian plots of the electron density. (B) Vertical excitation energies and relative energies of H_3^+ at, respectively, $D_{\infty h}$ and D_{3h} symmetries. (C) Magnetically induced ring currents for the 2^1A_1 and 1^1B_2 states which stem from the $1^1E'$ states upon geometric distortions to C_{2v} symmetric structures. The scaling factors reflect how large this distortion was (the value 1.0 represents the H–H bond lengths of the S_0 equilibrium geometry). The C_2 -axis indicates distortions in the direction of forming an acute isosceles triangle (moving H1 atom) and the x -axis distortions along an obtuse isosceles triangle formation (increasing the separation between H2 and H3).

excitation energy as their combined effects amount to 5.95 eV (Fig. 4B). The corresponding sum for the lowest triplet states is 7.50 eV. Both energies are in line with GSA-to-ESAA switches in character upon vertical excitation (Fig. 2).

Yet, the potential excited state antiaromatic character also needs to be probed through electronic and magnetic (anti)-aromaticity descriptors. With regard to the electron densities of these lowest excited states and their Laplacians, they exhibit significant differences from those of S_0 , which corroborates the loss of aromaticity upon excitation (Fig. 4A). Despite the D_{3h} symmetric geometry of H_3^+ in its vertically excited states, the electron density distribution has lower symmetry as it shifts toward the outer part of the atoms, preceding the dissociations that occur upon excitation to these states. Although the H atoms are still covalently bonded, as indicated by the value of the DIs, the 2^1A_1 and 1^1B_2 states exhibit drastic reductions of the three-center delocalization to 37–39% of the MCI value of S_0 (Fig. 4A). Similar conclusions can be reached on the antiaromaticity of

the $1^3E'$ (1^3A_1 and 1^3B_2) states based on the analysis of the electron delocalization in Fig. S2.⁵⁴ Thus, the $MCI^{1/n}$ values for H_3^+ (0.62 (S_0)), 0.46 and 0.45 ($1^1E'$), and 0.39 and 0.36 ($1^3E'$)), are comparable to those of benzene in its S_0 , S_1 , and T_1 states (0.59, 0.40, and 0.36, respectively).⁵⁵ This is consistent with an aromatic S_0 state, while the lowest excited singlet and triplet states ($1^1E'$ and $1^3E'$) are antiaromatic.

Going to the magnetic aspect of excited state antiaromaticity, the values of the magnetically induced ring currents obtained for the vertically excited $1^1E'$ states at the S_0 equilibrium geometry diverge as a result of the two-fold degeneracy at D_{3h} symmetry. The analysis of ring current strength at the C_{2v} symmetric structures reveals that the $1^1E'$ states exhibit a pole in the ring current at D_{3h} symmetric geometries (Fig. 4C), *i.e.*, a sudden change from highly diatropic to highly paratropic values, which explains the divergence observed at the vertical excitation. This resembles recent observations on the transient antiaromatic states of the c- C_{16} molecule where small bond length alterations lead to changes

from dia- to paratropicity, or *vice versa*,⁵⁷ related to the orbital degeneracies at highly symmetric structures.⁵⁸ Now, by following the C_{2v} symmetric dissociation paths of H_3^+ , and thus, the 2^1A_1 and 1^1B_2 states, we observe gradually diminishing paratropic ring currents (Fig. 4C), in line with antiaromaticity relief. Also the NICS(0)_{zz} values computed along these paths reveal antiaromaticity, with values of 77.1 and 84.7 ppm at two C_{2v} symmetric structures distorted by a factor 1.5, leading to, respectively, acute and obtuse isosceles triangular structures as exemplified in Fig. 3B (see further Section S3).

Protons-to-electrons ratios and impacts

Having established the antiaromaticity of the $1^1E'$ states of H_3^+ , the question is if the GSA-to-ESAA switch in character (Fig. 2) explains the unusually high vertical excitation energy of this cation. From computations of light atoms, molecules and ions with only two electrons such as He, Li^+ , HHe^+ and He_2^{2+} (Table S3), we see that high vertical excitation energies are characteristic of these species, which mostly cannot exhibit aromaticity as they are acyclic. Many of these ions are also found in space, *e.g.*, Li^+ and HHe^+ .⁵⁹ Indeed, it has been argued that HHe^+ was the first molecule of the Universe,^{60,61} and it produces H_2^+ upon collision with atomic H, which in turn can produce H_3^+ in a reaction with H_2 .⁶²

The excitation energies are higher for more positively charged species, and is highest when the protons are concentrated in one nucleus (He, Li^+ and Be^{2+}). Hence, in the $3p, 2e$ series, Li^+ and HHe^+ feature higher vertical $E(S_1)$ than H_3^+ by, respectively, 41.16 and 6.91 eV, and similar for the vertical $E(T_1)$ (Table S3). For the 2e species He, Li^+ and Be^{2+} , with protons-to-electrons ratios of 1.0, 1.5 and 2.0, respectively, the first excitation energy goes up dramatically from 20.94 eV to 60.44 eV and 121.26 eV as the excitation implies a gradually larger loss in the electrostatic attraction between electrons and nuclei.

Next, to estimate the impact of the protons-to-electrons ratio on the excitation energies, we explored the π -conjugated and S_0 aromatic cyclopropenium cation, $c-C_3H_3^+$, which has an equilateral triangular structure and a near-unit ratio of 1.05 between total nuclear and electronic charges (+21 *vs.* -20) (Sections S4 and S5).⁶³⁻⁶⁵ Indeed, $c-C_3H_3^+$ is isolobal with H_3^+ , *i.e.*, its π -orbitals are analogous to the σ -orbitals of H_3^+ .⁶⁶ Thus, this cation helps us decipher the relative contributions of the protons-to-electrons ratio *versus* the GSA-to-ESAA switch to the 19.28 eV excitation energy of H_3^+ .

The vertical transition to the lowest $\pi\pi^*$ states ($1^1E''$) of $c-C_3H_3^+$ requires 9.71 eV. This is only half that of the transition to the $\sigma\sigma^*$ states of H_3^+ but significantly higher than the lowest $\pi\pi^*$ states of any other π -bonded hydrocarbon, *e.g.*, 7.11 eV for ethylene.⁶⁷ Thus, $c-C_3H_3^+$ has its lowest $\pi\pi^*$ states at an unusually high excitation energy despite its near-unit protons-to-electrons ratio. Interestingly, there are several $\sigma\pi^*$ and $\pi\sigma^*$ states below the first $\pi\pi^*$ state. Therefore, the high excitation energy of the lowest $\pi\pi^*$ transition of $c-C_3H_3^+$ is not caused by a drastically diminished electrostatic attraction upon excitation. Instead, it should arise from the stabilization in the S_0 state due to aromaticity plus destabilization in the $\pi\pi^*$ states due to antiaromaticity, and this

applies also to the lowest triplet states. From this, one can estimate that the additional energy (9.57 eV) to reach the excitation energy of H_3^+ is caused by the electrostatic effect.

Also Li_3^+ , valence isoelectronic to H_3^+ , is an equilateral triangle at its global minimum in the S_0 state, but it is nonaromatic and best described as the smallest triatomic molecule with metallic bonding.⁸ We now find its lowest singlet excited states, the degenerate 1^1E states, at an energy of merely 2.70 eV. In line with the nonaromatic S_0 state, these states are also nonaromatic (see Table S3 and Section S6 in the SI). Compression to a triangle with half the Li-Li distance leads to no substantial changes in neither the singlet excitation energy nor the electron-nucleus attraction contributions (Table S3). Among the two possible mixed Li and H monocations (H_2Li^+ and HLi_2^+), H_2Li^+ has an acute triangular structure with Li-H and H-H distances of 2.049 and 0.752, respectively (Fig. S7). HLi_2^+ , on the other hand, has a linear structure⁶⁸ and was therefore not further considered here as it is nonaromatic.

Finally, H_2He^{2+} is also interesting in this context as it provides an electronegativity perturbation compared to the isoelectronic H_3^+ ,⁵⁹ although our computations reveal that this dication is not a minimum on the S_0 PES. However, when kept at the geometry which is optimal for H_3^+ but with one H^+ exchanged to He^{2+} , we find that it is nonaromatic in both its S_0 state and lowest singlet excited states (Fig. S10). Accordingly, there is no GSA-to-ESAA switch in character upon the excitation of H_2He^{2+} . In line with this, there is no significant increase in excitation energy (+0.24 eV) when going from HHe^+ to H_2He^{2+} , in contrast to what is observed when going from H_2 to H_3^+ (+6.56 eV, see Table S3 and Section S6 for further discussion).

Comparisons to analogous carbocations

Further analysis of the $c-C_3H_3^+$ cation, a molecular ion which also is of astrochemical importance,²⁹ enables us to show that the very high first excitation energy of H_3^+ is due to both stabilization by GSA plus destabilization by ESAA and the high protons-to-electrons ratio. Among the (anti)aromaticity aspects, we thus first explore the energetic aspect before the electronic and magnetic ones. The isomerization stabilization energy (ISE)⁶⁹ of $c-C_3H_3^+$ in S_0 , computed as the reaction energy for the 1,3-hydrogen shift from a nonaromatic isomer to the S_0 aromatic methylcyclopropenium cation (Fig. 5A), is -2.03 eV with CCSD. This reveals a stronger aromatic character than that of benzene in S_0 (-1.34 eV with CCSD/aug-cc-pVDZ). In contrast, the lowest vertically excited singlet and triplet $\pi\pi^*$ states exhibit large positive ISE values of 2.66 and 2.78 eV with EOM-CCSD, corresponding to strong excited state antiaromatic destabilization. Accordingly, the S_0 stabilization plus excited state antiaromatic destabilizations of $c-C_3H_3^+$ are 4.69 and 4.81 eV, respectively, and these should represent lower bounds for the analogous energies in H_3^+ .

A comparison of the various energies of the linear H_3^+ with the corresponding ones of the allyl cation ($H_2CCHCH_2^+$) allows for a second estimate of the impact of the high protons-to-electrons ratio of H_3^+ . The two species are isolobal and nonaromatic in S_0 , yet, have different protons-to-electrons counts (3 : 2 *vs.* 23 : 22). For the allyl cation, with a near-unit protons-to-



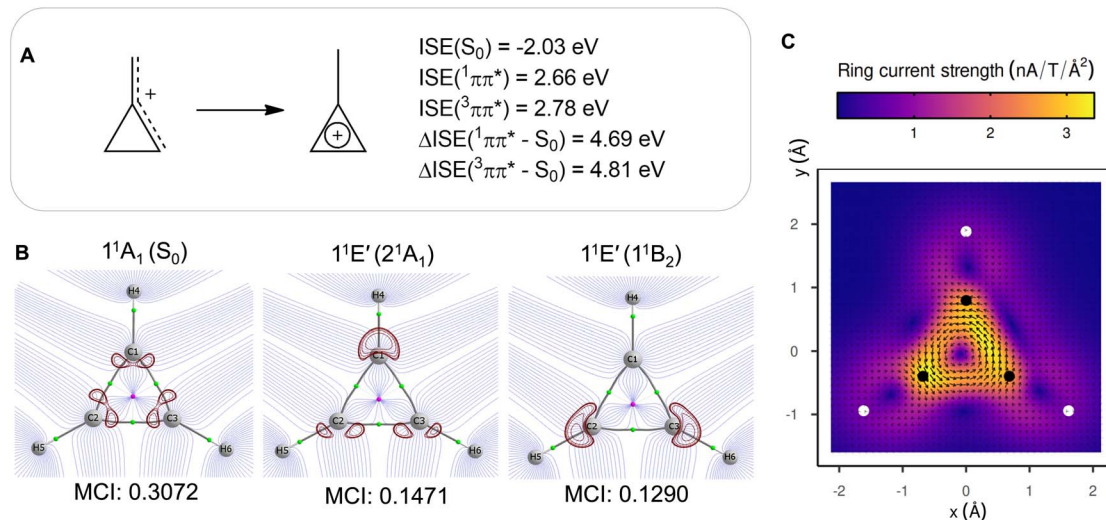


Fig. 5 (A) Isomerization stabilization energies (ISEs) of the methylcyclopropenium cation in the S_0 and lowest vertically excited singlet and triplet $\pi\pi^*$ states, and the combined ISEs. (B) Topological analysis and Laplacian of the electron density (red) of S_0 and excited states of $c\text{-C}_3\text{H}_3^+$ at its S_0 geometry (1.0 a.u. above ring plane) and MCI values. (C) MICD of the cyclopropenium cation in its $1^1E''$ (1^1B_2) state vertically excited from S_0 showing paratropic (antiaromatic) ring currents (1.0 a.u. above ring plane). Carbon atoms plotted as black balls and hydrogen atoms as white.

electrons ratio, the lowest vertical $\pi\pi^*$ singlet state is found at 5.50 eV, while the first $\sigma\sigma^*$ excitation energy of linear H_3^+ is 13.33 eV, *i.e.*, 7.83 eV higher than that of the allyl cation. Both this and the excitation energy difference between $c\text{-C}_3\text{H}_3^+$ and H_3^+ (9.57 eV) provide estimates of the electrostatic contribution to excitation energies of H_3^+ (Fig. 6).

Antiaromaticity assessments of $c\text{-C}_3\text{H}_3^+$ in its first singlet excited $\pi\pi^*$ state by usage of electronic and magnetic descriptors reveal a clear resemblance to H_3^+ . The MCI values demonstrate their electronic structural similarities with the values for, respectively, the $1^1E'$ and $1^1E''$ states being less than half those of the S_0 state (Fig. 4 and 5B), and this is further emphasized by the topological analysis of their excited state electronic structures (Fig. 4A and 5B). Finally, the MICD of the cyclopropenium cation in its lowest $\pi\pi^*$ state reveals a paratropic (antiaromatic) ring current in the three-membered ring (Fig. 5C), similar as for the two dissociation pathways of H_3^+ (Fig. 4C). Furthermore, and as described above, the antiaromatic character of the lowest $\pi\pi^*$ states, leading to an extreme destabilization, should be a strongly contributing factor to these states not being the lowest excited states of $c\text{-C}_3\text{H}_3^+$. In contrast, for the allyl cation the lowest $\pi\pi^*$ state is the S_1 state. As photochemical reactions normally proceed from the lowest electronically excited state according to Kasha's rule, this will impact on the photochemistry of the $c\text{-C}_3\text{H}_3^+$ and its alkyl substituted derivatives, likely leading to reduced photoreactivities when compared to species where $\pi\pi^*$ states are the lowest excited states.

Thus, $c\text{-C}_3\text{H}_3^+$ like H_3^+ , exhibit strong aromaticity in the S_0 state and strong antiaromaticity in, respectively, the lowest $\pi\pi^*$ and $\sigma\sigma^*$ excited states, yet the excitation energy of the latter is additionally affected by a high protons-to-electrons ratio. Indeed, by adding energy additives to the lowest excitation energy of the acyclic and nonaromatic allyl cation (5.50 eV) one can estimate the excitation energy of H_3^+ (Fig. 6). The energy for

the GSA-to-ESAA switch in character in $c\text{-C}_3\text{H}_3^+$ (4.69 eV) or the extra cyclic resonance energy of H_3^+ (5.95 eV), and the excitation energy difference between the allyl cation and linear H_3^+ or between triangular $c\text{-C}_3\text{H}_3^+$ and H_3^+ (7.83–9.57 eV), as measures of the electrostatic energy loss between protons and electrons upon excitation, added to 5.50 eV gives 18.0–21.0 eV (Fig. 6). This energy range brackets our computed first excitation energy of H_3^+ of 19.28 eV. It also becomes clear that it is the GSA-to-ESAA switch in character which places the first singlet excited

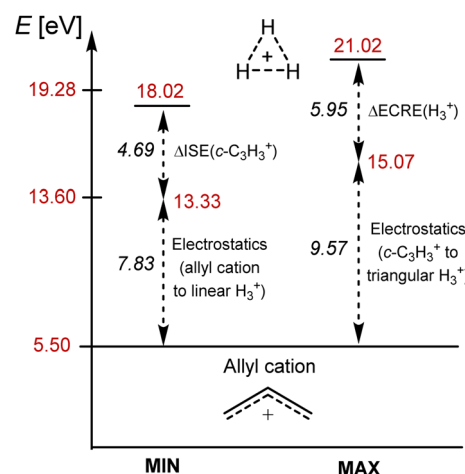


Fig. 6 Estimation of the minimum and maximum of the excitation energy of triangular H_3^+ with the first $\pi\pi^*$ excitation energy of the allyl cation as the starting point, to which energy additives representing two types of components are added: (i) the difference in electrostatics upon excitation due to different protons-to-electrons ratio in the carbocations and H_3^+ , and (ii) the GSA-to-ESAA switch in character upon excitation. ΔISE = difference in isomerization stabilization energy between the S_0 and lowest $\pi\pi^*$ excited state of $c\text{-C}_3\text{H}_3^+$, and $\Delta ECRE$ = difference in extra cyclic resonance energy between the S_0 and $\sigma\sigma^*$ states of H_3^+ .

states well above the ionization energy of monohydrogen, and thus, provides H_3^+ with its astrophotocchemical persistence.

Conclusions

Herein, we decipher the main causes of the very high electronic excitation energy of H_3^+ , which enables its functions in space. This is achieved through a comparison of triangular H_3^+ and linear H_3^+ with two analogous π -conjugated hydrocarbon ions, the cyclopropenium cation ($\text{c-C}_3\text{H}_3^+$) and the allyl cation ($\text{CH}_2^-\text{CHCH}_2^+$). Had the vertical excitation energy been lower (closer to the photoionization of the much more abundant monohydrogen), H_3^+ would have been more prone to photodissociate in space. We reveal that three factors contribute to the high excitation energy; (i) the change from a stabilizing aromatic character to (ii) a destabilizing antiaromatic character upon excitation from S_0 to the lowest excited states (present also in $\text{c-C}_3\text{H}_3^+$), and (iii) the high ratio between total nuclear and electronic charges (which is present also in small cations). These three factors together provide the origin of the astrophotocchemical inertness of H_3^+ . Without this photostability, H_3^+ could not have had the functions it has in the Universe, which would have led to a Universe different from the one we know. Furthermore, it may also impact on the photostability of species with similar 3-center-2-electron bonding characteristics as the H_3^+ ion, such as the vinyl and ethyl cations (C_2H_3^+ and C_2H_5^+ , respectively),^{29–31,70} as well as the S_0 state aromatic $\text{c-C}_3\text{H}_3^+$ and derivatives, which are all of astrochemical importance.^{29,70} The excited state dynamics of these carbocationic species are not extensively explored but it can be an important direction for future research in astrochemistry.

We show for the first time that excited state antiaromaticity is a molecular electronic structure property with crucial astrochemical influence that also has astrophysical implications. In a broader sense, our findings point to the roles of excited state aromaticity and antiaromaticity as important new concepts for interpretation in astrochemistry. We anticipate that these effects impact on a number of photochemical processes in space.

Computational methods

Geometry and energy calculations

Geometry optimizations and energy calculations were performed with Gaussian 16 revision C.01.⁷¹ The electronic singlet ground state and lowest excited triplet state were calculated using CCSD while singlet excited states were computed with EOM-CCSD. For H_3^+ , this level is equivalent to full configuration interaction (FCI), and we referred to it as FCI in the manuscript. Frequency calculations were performed at the same level of theory to probe if the structures were minima or saddle points on the potential energy surfaces. In all cases, the aug-cc-pVTZ valence triplet-zeta of Dunning and co-workers⁷² was used as the basis set. For wavefunction analysis we employed 6d 10f functions for the latter basis set. To obtain T_2 state the orbital order was altered by usage of the guess = alter keyword in Gaussian. Calculations of electron–nucleus attraction contribution include core electrons for all molecules (see Table S3).

Aromaticity assessment

Results of the multicentre index (MCI)⁵³ were computed by usage of AIMAll,⁷³ APOST-3D, and ESI-3D^{56,74} packages. Due to the presence of a non-nuclear attractor (NNA) in some of the species, we consider a different partition of the molecular space to compute the delocalization indices (DI(F))^{51,52} and the MCI. Some of us have previously found that Becke-rho's atomic partition provides similar values to partitions based on quantum theory of atoms in molecules (QTAIM),⁷⁵ a theory which uses a topological approach to define an atom in a molecule. Becke's partition employs the position of the bond critical points (BCP) between atoms to define the atomic radii in the original Becke's partition.⁷⁶ This multicentre integration technique assigns weights to atoms in the molecule. The calculation of the DI for correlated wavefunctions employed the so-called Fulton approximation,⁷⁷ which provides very good agreement with the actual DI.

Isomerization stabilization energies (ISE) were computed at (EOM)-CCSD/cc-pVTZ optimized geometries but for the energy values reported we used the aug-cc-pVTZ basis set.

The magnetically induced ring current density (MICD) was calculated by employing complete active space self-consistent field (CASSCF) method (with all electrons, and occupied and virtual orbitals included in the active space, corresponding to an FCI calculation) and aug-cc-pVTZ basis set, using a development version of Dalton Program 2020.^{78,79} In order to compute the ring current passing through the bonds of the triangular H_3^+ , the MICD was integrated in a plane perpendicular to the bond, spanning from the centre of mass of the molecule 20 bohr at opposite sides of the plane (along vectors normal to the ring plane and cutting through the bond) using 200 subdivisions in the Gauss–Lobatto quadrature.⁸⁰

Author contributions

Conceptualization: HO; methodology: HO, CFN, EM; investigation: JMT, JKS; visualization: JMT, JKS; funding acquisition: HO; project administration: HO; supervision: HO; analysis: JMT, JKS; writing – original draft: JMT; writing – review & editing: JMT, JKS, EM, CFN, HO.

Conflicts of interest

There are no conflicts to declare.

Data availability

The data underlying this study are openly available in the published article and its supplementary information (SI), and also openly available in zenodo at <https://doi.org/10.5281/zenodo.15713452>. The data supporting this article have been included as part of the SI. Supplementary information: Section S1: energies and geometries of H_3^+ ; Section S2: aromaticity of H_3^+ , electronic properties; Section S3: aromaticity of H_3^+ , magnetic properties; Section S4: protons-to-electrons ratios; Section S5: cyclopropenium cation (C_3H_3^+);

Section S6: Li_3^+ , H_2Li^+ and H_2He^{2+} ; Section S7: supplementary references; Section S8: Cartesian coordinates, absolute energies, and imaginary frequencies for all calculated structures. See DOI: <https://doi.org/10.1039/d5sc09067a>.

Acknowledgements

We thank Dr Radovan Bast for extensive help with the magnetically induced current density calculations, Mr Hannes Gustafsson and Dr Lucia Corti for involvement in preliminary calculations. We also thank Prof. Jochen Autschbach, Prof. Paul Barklem, Prof. Eszter Borbas, Prof. em. Bengt Gustafsson, Prof. Martin Rahm, Prof. Philippe Wernet, and Prof. Judy Wu for discussions on the project at various stages. The computations were enabled by resources provided by the National Academic Infrastructure for Supercomputing in Sweden (NAISS) and the Swedish National Infrastructure for Computing (SNIC) at the National Supercomputer Center (NSC), Linköping, Sweden, through grant agreements 2022/5-378, 2023/5-335 and 2024/5-422. The Foundation Olle Engkvist Byggmästare is greatly acknowledged for a postdoctoral fellowship to J. M. T. (grant 184-390). H. O. thanks the Swedish Research Council for financial support (grants 2019-05618 and 2023-04179), and J. M. T. thanks the University Claude Bernard Lyon 1 for the funding provided through AAP Accueil EC. E. M. is grateful for the funding and technical support provided by the Donostia FEDER Una manera de hacer Europa International Physics Center (DIPC), and grant PID2022-140666NB-C21 funded by MCIN/AEI/10.13039/501100011033 and “FEDER Una manera de hacer Europa”. C. F.-N. thanks National Science Centre, Poland 2020/39/B/ST4/02022 for funding.

References

- 1 T. Oka, *Chem. Rev.*, 2013, **113**, 8738–8761.
- 2 T. R. Geballe and T. Oka, *Nature*, 1996, **384**, 334–335.
- 3 M. Larsson, *Int. J. Astrobiol.*, 2008, **7**, 237–241.
- 4 S. Miller, T. Stallard, H. Melin and J. Tennyson, *Faraday Discuss.*, 2010, **147**, 283–291.
- 5 G. Kannan, J. R. Chien, A. J. Benjamin, N. Bhatia and R. J. Saykally, *J. Phys. Chem. A*, 2021, **125**, 4267–4275.
- 6 R. W. A. Havenith, F. De Proft, P. W. Fowler and P. Geerlings, *Chem. Phys. Lett.*, 2005, **407**, 391–396.
- 7 S. Sadjadi, *Struct. Chem.*, 2017, **28**, 1445–1452.
- 8 C. Foroutan-Nejad and P. Rashidi-Ranjbar, *J. Mol. Struct. THEOCHEM*, 2009, **901**, 243–248.
- 9 D. Zhao, X. He, M. Li, C. Guo, C. Rong, P. K. Chattaraj and S. Liu, in *Atomic Clusters with Unusual Structure, Bonding and Reactivity*, ed. P. K. Chattaraj, S. Pan and G. Merino, Elsevier, 2023, pp. 237–245, DOI: [10.1016/B978-0-12-822943-9.00017-6](https://doi.org/10.1016/B978-0-12-822943-9.00017-6).
- 10 M. Solà, A. I. Boldyrev, M. K. Cyrański, T. M. Krygowski and G. Merino, *Aromaticity and antiaromaticity: Concepts and applications*, John Wiley & Sons, Ltd, 2023.
- 11 M. Pavanello and L. Adamowicz, *J. Chem. Phys.*, 2009, **130**, 034104.
- 12 A. Petignani, D. Bing, O. Novotný, M. H. Berg, H. Buhr, M. Grieser, B. Jordon-Thaden, C. Krantz, M. B. Mendes, S. Menk, S. Novotny, D. A. Orlov, R. Repnow, J. Stützel, X. Urbain and A. Wolf, *J. Phys. Chem. A*, 2010, **114**, 4864–4869.
- 13 X. Urbain, A. Dochain, R. Marion, T. Launoy and J. Loreau, *Philos. Trans. R. Soc., A*, 2019, **377**, 20180399.
- 14 K. Kawaoka and R. F. Borkman, *J. Chem. Phys.*, 1971, **54**, 4234–4238.
- 15 E. v. Dishoeck and H. R. Hrodmarsson, Leiden photodissociation and photoionization cross section database, https://home.strw.leidenuniv.nl/~ewine/photo/display_h3+_f8a0eca1bcc94c898fc68220d4b45be8.html, accessed 10/25, 2024.
- 16 H. R. Hrodmarsson and E. F. van Dishoeck, *Astron. Astrophys.*, 2023, **675**, A25.
- 17 A. N. Heays, A. D. Bosman and E. F. van Dishoeck, *Astron. Astrophys.*, 2017, **602**, A105.
- 18 S. Lepp, P. C. Stancil and A. Dalgarno, *J. Phys. B: At., Mol. Opt. Phys.*, 2002, **35**, R57.
- 19 E. F. van Dishoeck, *Symp. – Int. Astron. Union*, 1987, **120**, 51–65.
- 20 D. Galli and F. Palla, *Annu. Rev. Astron. Astrophys.*, 2013, **51**, 163–206.
- 21 L. Adamowicz and M. Pavanello, *Philos. Trans. R. Soc., A*, 2012, **370**, 5001–5013.
- 22 A. V. Turbiner and J. C. Lopez Vieyra, *J. Phys. Chem. A*, 2013, **117**, 10119–10128.
- 23 J. Tennyson, O. L. Polyansky, N. F. Zobov, A. Alijah and A. G. Császár, *J. Phys. B: At., Mol. Opt. Phys.*, 2017, **50**, 232001.
- 24 N. C. Baird, *J. Am. Chem. Soc.*, 1972, **94**, 4941–4948.
- 25 M. Rosenberg, C. Dahlstrand, K. Kilså and H. Ottosson, *Chem. Rev.*, 2014, **114**, 5379–5425.
- 26 R. Papadakis and H. Ottosson, *Chem. Soc. Rev.*, 2015, **44**, 6472–6493.
- 27 J. Kim, J. Oh, A. Osuka and D. Kim, *Chem. Soc. Rev.*, 2022, **51**, 268–292.
- 28 J. Yan, T. Slanina, J. Bergman and H. Ottosson, *Chem.-Eur. J.*, 2023, **29**, e202203748.
- 29 A. Ali, E. C. Sittler, D. Chornay, B. R. Rowe and C. Puzzarini, *Planet. Space Sci.*, 2013, **87**, 96–105.
- 30 C. M. Gabrys, D. Uy, M. F. Jagod, T. Oka and T. Amano, *J. Phys. Chem.*, 1995, **99**, 15611–15623.
- 31 G. E. Doublerly, A. M. Ricks, B. W. Ticknor, W. C. McKee, P. v. R. Schleyer and M. A. Duncan, *J. Phys. Chem. A*, 2008, **112**, 1897–1906.
- 32 B. Żurawski, R. Ahlrichs and W. Kutzelnigg, *Chem. Phys. Lett.*, 1973, **21**, 309–313.
- 33 R. Beckmann, R. Topolnicki and D. Marx, *J. Phys. Chem. A*, 2023, **127**, 2460–2471.
- 34 H. S. Andrei, N. Solcà and O. Dopfer, *Angew. Chem.*, 2007, **120**, 401–403.
- 35 P. C. Varras, M. G. Siskos and P. S. Gritzapis, *Mol. Phys.*, 2020, **118**, e1706778.
- 36 B. T. Psciuik, V. A. Benderskii and H. B. Schlegel, *Theor. Chem. Acc.*, 2007, **118**, 75–80.
- 37 R. C. Fortenberry, X. Huang, T. D. Crawford and T. J. Lee, *J. Phys. Chem. A*, 2014, **118**, 7034–7043.
- 38 A. Ali, E. C. Sittler, D. Chornay, B. R. Rowe and C. Puzzarini, *Planet. Space Sci.*, 2015, **109–110**, 46–63.



39 G. A. Olah, T. Mathew, G. K. S. Prakash and G. Rasul, *J. Am. Chem. Soc.*, 2016, **138**, 1717–1722.

40 H. A. Jahn and E. Teller, *Proc. R. Soc. London, Ser. A*, 1937, **161**, 220–235.

41 M. Pavanello, W. C. Tung, F. Leonarski and L. Adamowicz, *J. Chem. Phys.*, 2009, **130**, 074105.

42 B. Mukherjee, S. Mukherjee and S. Adhikari, *J. Phys.: Conf. Ser.*, 2016, **759**, 012050.

43 Z. Peng, S. Kristyan, A. Kuppermann and J. S. Wright, *Phys. Rev. A*, 1995, **52**, 1005–1023.

44 P. Barragán, L. F. Errea, A. Macías, L. Méndez, I. Rabadán and A. Riera, *J. Chem. Phys.*, 2006, **124**, 184303.

45 S. Mukherjee, D. Mukhopadhyay and S. Adhikari, *J. Chem. Phys.*, 2014, **141**, 204306.

46 A. Znotins, F. Grussie, A. Wolf, X. Urbain and H. Kreckel, *J. Mol. Spectrosc.*, 2021, **378**, 111476.

47 L. J. Schaad and W. V. Hicks, *J. Chem. Phys.*, 1974, **61**, 1934–1942.

48 Y. Mo and P. v. R. Schleyer, *Chem.-Eur. J.*, 2006, **12**, 2009–2020.

49 X. Lin and Y. Mo, *Angew. Chem. Int. Ed. Engl.*, 2022, **61**, e202209658.

50 F. Feixas, E. Matito, J. Poater and M. Solà, *Chem. Soc. Rev.*, 2015, **44**, 6434–6451.

51 R. F. W. Bader and M. E. Stephens, *Chem. Phys. Lett.*, 1974, **26**, 445–449.

52 R. F. W. Bader and M. E. Stephens, *J. Am. Chem. Soc.*, 1975, **97**, 7391–7399.

53 P. Bultinck, R. Ponec and S. Van Damme, *J. Phys. Org. Chem.*, 2005, **18**, 706–718.

54 E. Matito, *Phys. Chem. Chem. Phys.*, 2016, **18**, 11839–11846.

55 F. Feixas, J. Vandenbussche, P. Bultinck, E. Matito and M. Solà, *Phys. Chem. Chem. Phys.*, 2011, **13**, 20690–20703.

56 E. Matito, M. Solà, P. Salvador and M. Duran, *Faraday Discuss.*, 2007, **135**, 325–345.

57 I. Rončević, F. J. Leslie, M. Rossmannek, I. Tavernelli, L. Gross and H. L. Anderson, *J. Am. Chem. Soc.*, 2023, **145**, 26962–26972.

58 E. Steiner and P. W. Fowler, *J. Phys. Chem. A*, 2001, **105**, 9553–9562.

59 L. González-Sánchez, N. Sathyamurthy and F. A. Gianturco, *Phys. Chem. Chem. Phys.*, 2023, **25**, 23370–23383.

60 R. Güsten, H. Wiesemeyer, D. Neufeld, K. M. Menten, U. U. Graf, K. Jacobs, B. Klein, O. Ricken, C. Risacher and J. Stutzki, *Nature*, 2019, **568**, 357–359.

61 R. C. Fortenberry, *Chem.*, 2019, **5**, 1028–1030.

62 Y. Mi, E. Wang, Z. Dube, T. Wang, A. Y. Naumov, D. M. Villeneuve, P. B. Corkum and A. Staudte, *Nat. Chem.*, 2023, **15**, 1224–1228.

63 R. Breslow, J. T. Groves and G. Ryan, *J. Am. Chem. Soc.*, 1967, **89**, 5048.

64 M. N. Glukhovtsev, S. Laiter and A. Pross, *J. Phys. Chem.*, 1996, **100**, 17801–17806.

65 K. B. Wiberg and P. R. Rablen, *J. Org. Chem.*, 2020, **85**, 11741–11749.

66 R. Hoffmann, *Angew. Chem., Int. Ed.*, 1982, **21**, 711–724.

67 R. S. Mulliken, *J. Chem. Phys.*, 1977, **66**, 2448–2451.

68 B. H. Cardelino, W. H. Eberhardt and R. F. Borkman, *J. Chem. Phys.*, 1986, **84**, 3230–3242.

69 P. v. R. Schleyer and F. Pühlhofer, *Org. Lett.*, 2002, **4**, 2873–2876.

70 G. A. Olah, *J. Am. Chem. Soc.*, 1972, **94**, 808–820.

71 M. J. Frisch, G. W. Trucks, H. B. Schlegel, G. E. Scuseria, M. A. Robb, J. R. Cheeseman, G. Scalmani, V. Barone, G. A. Petersson, H. Nakatsuji, X. Li, M. Caricato, A. V. Marenich, J. Bloino, B. G. Janesko, R. Gomperts, B. Mennucci, H. P. Hratchian, J. V. Ortiz, A. F. Izmaylov, J. L. Sonnenberg, D. Williams, F. Ding, F. Lipparini, F. Egidi, J. Goings, B. Peng, A. Petrone, T. Henderson, D. Ranasinghe, V. G. Zakrzewski, J. Gao, N. Rega, G. Zheng, W. Liang, M. Hada, M. Ehara, K. Toyota, R. Fukuda, J. Hasegawa, M. Ishida, T. Nakajima, Y. Honda, O. Kitao, H. Nakai, T. Vreven, K. Throssell, J. A. Montgomery Jr, J. E. Peralta, F. Ogliaro, M. J. Bearpark, J. J. Heyd, E. N. Brothers, K. N. Kudin, V. N. Staroverov, T. A. Keith, R. Kobayashi, J. Normand, K. Raghavachari, A. P. Rendell, J. C. Burant, S. S. Iyengar, J. Tomasi, M. Cossi, J. M. Millam, M. Klene, C. Adamo, R. Cammi, J. W. Ochterski, R. L. Martin, K. Morokuma, O. Farkas, J. B. Foresman and D. J. Fox, *Gaussian 16, Revision C.01*, Gaussian, Inc., Wallington CT, 2016.

72 D. E. Woon and T. H. Dunning Jr, *J. Chem. Phys.*, 1993, **98**, 1358–1371.

73 T. A. Keith, *TK Gristmill Software*, Overland Park KS, USA, 2019.

74 E. Matito, *IQCC (Girona, Catalonia) and DIPC (Donostia, Euskadi)*, Spain 2015.

75 R. F. W. Bader, *Atoms in molecules : a quantum theory*, Clarendon press, Oxford, 1990.

76 A. D. Becke, *J. Chem. Phys.*, 1988, **88**, 2547–2553.

77 R. L. Fulton, *J. Phys. Chem.*, 1993, **97**, 7516–7529.

78 K. Aidas, C. Angeli, K. L. Bak, V. Bakken, R. Bast, L. Boman, O. Christiansen, R. Cimiraglia, S. Coriani, P. Dahle, E. K. Dalskov, U. Ekström, T. Enevoldsen, J. J. Eriksen, P. Ettenhuber, B. Fernández, L. Ferrighi, H. Fliegl, L. Frediani, K. Hald, A. Halkier, C. Hättig, H. Heiberg, T. Helgaker, A. C. Hennum, H. Hettema, E. Hjertenæs, S. Høst, I. M. Høyvik, M. F. Iozzi, B. Jansík, H. J. Jensen, D. Jonsson, P. Jørgensen, J. Kauczor, S. Kirpekar, T. Kjærgaard, W. Klopper, S. Knecht, R. Kobayashi, H. Koch, J. Kongsted, A. Krapp, K. Kristensen, A. Ligabue, O. B. Lutnæs, J. I. Melo, K. V. Mikkelsen, R. H. Myhre, C. Neiss, C. B. Nielsen, P. Norman, J. Olsen, J. M. Olsen, A. Osted, M. J. Packer, F. Pawłowski, T. B. Pedersen, P. F. Provasi, S. Reine, Z. Rinkevicius, T. A. Ruden, K. Ruud, V. V. Rybkin, P. Sałek, C. C. Samson, A. S. de Merás, T. Saue, S. P. Sauer, B. Schimmelpfennig, K. Sneskov, A. H. Steindal, K. O. Sylvester-Hvid, P. R. Taylor, A. M. Teale, E. I. Tellgren, D. P. Tew, A. J. Thorvaldsen, L. Thøgersen, O. Vahtras, M. A. Watson, D. J. Wilson, M. Ziolkowski and H. Agren, *Wiley Interdiscip. Rev.: Comput. Mol. Sci.*, 2014, **4**, 269–284.

79 G. Ganguly, S. Pathak and A. Paul, *Phys. Chem. Chem. Phys.*, 2021, **23**, 16005–16012.

80 J. Jusélius, D. Sundholm and J. Gauss, *J. Chem. Phys.*, 2004, **121**, 3952–3963.

